07 - 10 September 2009

PROCEEDINGS

54. IWK

Internationales Wissenschaftliches Kolloquium
International Scientific Colloquium

Information Technology and Electrical Engineering - Devices and Systems, Materials and Technologies for the Future

Faculty of Electrical Engineering and Information Technology

Startseite / Index:
http://www.db-thueringen.de/servlets/DocumentServlet?id=14089

TECHNISCHE UNIVERSITÄT
ILMENAU

Impressum

Herausgeber: Der Rektor der Technischen Universität Ilmenau
Univ.-Prof. Dr. rer. nat. habil. Dr. h. c. Prof. h. c.
Peter Scharff

Redaktion: Referat Marketing
Andrea Schneider

Fakultät für Elektrotechnik und Informationstechnik
Univ.-Prof. Dr.-Ing. Frank Berger

Redaktionsschluss: 17. August 2009

Technische Realisierung (USB-Flash-Ausgabe):
Institut für Medientechnik an der TU Ilmenau
Dipl.-Ing. Christian Weigel
Dipl.-Ing. Helge Drumm

Technische Realisierung (Online-Ausgabe):
Universitätsbibliothek Ilmenau
ilmedia
Postfach 10 05 65
98684 Ilmenau

Verlag:
Verlag ISLE, Betriebsstätte des ISLE e.V.
Werner-von-Siemens-Str. 16
98693 Ilmenau

ISBN (USB-Flash-Ausgabe): 978-3-938843-45-1
ISBN (Druckausgabe der Kurzfassungen): 978-3-938843-44-4

Startseite / Index:
http://www.db-thueringen.de/servlets/DocumentServlet?id=14089

STRUCTURE AND RESISTIVITY OF FeCoZr-DIELECTRIC GRANULAR NANOCOMPOSITES SINTERED IN MIXED Ar+O_2 ATMOSPHERE

[1]J.Fedotova, Yu.Kasiuk[1], A.Larkin[1], J.Przewoznik[2], Cz.Kapusta[2], Yu.Kalinin[3]

[1]NCPHEP Belarusian State University, 220040 Minsk, Belarus
[2]AGH University of Science and Technology, 30-059 Cracow, Poland
[3]Voronez State University, 394006, Voronez, Russia

ABSTRACT

The response of structure, electrical conductivity, magnetoresistivity and magnetic properties of $(FeCoZr)_x(Al_2O_3)_{1-x}$ and $(FeCoZr)_X(PZT)_{100-X}$ (17 at. % < x < 67 at. %) nanocomposite films on oxygen incorporation into the sputtering ambient was investigated using Mössbauer spectroscopy, resistivity and magnetoresistivity measurements. Change of Fe local states and carrier transport mechanisms due to incorporation of oxygen into FeCoZr-containing granular nanocomposites (*GNCs*) with two different matrixes are discussed with regard to the formation of complex semiconductive FeCo-oxide interlayers and/or shells possessing different types of conductivity as well as the specific properties of Al_2O_3 and PZT.

Index Terms - One, two, three, four, five, six, seven, eight, nine, ten

1. INTRODUCTION

Unique magnetic and electroconductivity properties of granular soft ferromagnetic metal-dielectric matrix nanocomposite materials (*GNCs*) make them very attractive in designing of various magnetoelectronic devices [1-3]. It is well established now that for binary metal-dielectric *GNCs* electrical conductivity with and without applied external magnetic field should be considered within the frame of percolation theory [4]. It defines the percolation threshold X_C as such a concentration of metallic nanoparticles X_{FeCoZr} in *GNCs* when conductivity mechanism changes from tunnelling or variable-range hopping (VHR) to the metallic carrier transport due to formation of current-conductive cluster. Experimentally observed, that numerous characteristics of *GNCs*, like coercive force, magnetoresistivity effect, etc. revealed maximum values particularly within X_C [5]. The replacement of tunneling and/or VHR by localized states in dielectric with metallic conductivity through percolative net of nanoparticles has been experimentally observed within $X_C \approx 50$ % with some variations for different metallic and dielectric compositions. For the case of FeCoZr-Al_2O_3 sintered in pure Ar ambient experimentally established X_C was about 45-47 at. % of FeCoZr [6].

It is noteworthy that in some cases formation of current-conductive cluster of metallic nanoparticles within X_C coincide with nucleation of ferromagnetically-interacting net of metallic nanoparticles, although this is not the general case. In so doing, both magnetic and conductivity properties of *GNCs* are governed with X_{FeCoZr} value with respect to X_C for definite combination of metal and dielectric.

Previously obtained results of RT Mössbauer spectroscopy, SQUID-magnetometry and atomic force – magnetic force microscopy [6] confirmed that sputtering of FeCoZr-Al_2O_3 *GNC* in mixed Ar+O_2 ambient draw to drastic change of correspondent magnetic characteristics and structure. It was related to the progressive oxidation of FeCoZr nanoparticles with X_{FeCoZr} increase and also formation of complex FeCo-oxides.

Present research was focused on two main purposes: *(i)* to clarify the correlation between formed local Fe states in oxidized FeCoZr-Al_2O_3 *GNC* and correspondent electrical properties; *(ii)* to investigate the role of matrix in oxidation of FeCoZr as well as resistivity and magnetoresisitivity on the example of FeCoZr-$Pb_{0,81}Sr_{0,04}(NaBi)_{0,15}(ZrTi)O_3$ (doped PZT) *GNCs*. Application of segneto- and ferroelectric PZT matrix is supposed to be useful when varying state of *GNCs* by application of external magnetic or electric field.

2. EXPERIMENTAL

Nanogranular films of $(Fe_{45}Co_{45}Zr_{10})_x(D)_{100-x}$ (17 at.% < x < 67 at.%), where dielectric matrix D was either Al_2O_3 or $Pb_{0,81}Sr_{0,04}(Na_{0,5}Bi_{0,5})_{0,15}(Zr_{0,575}Ti_{0,425})O_3$ (doped PZT), were deposited on glass-ceramic and Al substrates by ion-beam sputtering in gas mixture Ar+O_2 atmosphere at partial oxygen pressures P_O = $2{,}4 \div 4{,}2 \cdot 10^{-3}$ Pa. The details of deposition procedure were summarized in [6].

Room temperature 57Fe Mössbauer spectroscopy was applied to reveal of local structure and magnetic state of the nanocomposites. The spectra were recorded at RT in transmission geometry using 57Co/Rh source (40 mCi). The fitting procedure was performed with the use of MOSMOD program assuming the distribution of hyperfine magnetic fields (H_{hf}) and quadrupole splittings (ε). All isomer shifts

(δ) were referenced to α-Fe. Lorentzian width (FWHM) of the fitted spectral lines was constant and equaled to 0.15 mm/s. Relatively high FWHM value was attributed to the amorphous structure of FeCoZr nanoparticles.

Mechanisms of carrier transport in *GNCs* were studied using temperature dependences of DC conductivity at the temperature range 4 – 300 K. To make these measurements, the nanocomposite films sputtered onto glass-ceramic substrates were cut into rectangular strips with dimensions of 10 mm × 2 mm × d μm (d is thickness of the films), and 4 indium contacts were deposited using ultrasound soldering. Samples were measured in flow cryostat system or closed-cycle refrigerator with electric field intensities E up to 10^5 V/m and magnetic fields with induction B up to 600 mT or 8 T using the 4 probe potentiometric method. Ratio error of electric conductance measurements was better than 5 %.

2.1. Mössbauer spectroscopy

Mössbauer spectra of the samples deposited at $P_O = 4.2 \cdot 10^{-3}$ Pa (see Fig. 1) show nonmagnetic behavior in the whole range of X_{FeCoZr}. It is in contrast with the results reported in [5,6], where spectra of FeCoZr-Al_2O_3 sintered in pure Ar ambient revealed the transition from nonmagnetic spectrum to magnetically split spectrum at $X_{FeCoZr} = X_C \approx 47$ at.%. Such transformation was assigned to the structural change from non-interacting superparamagnetic FeCoZr nanoparticles to the ferromagnetically interacting net of these nanoparticles.

Mössbauer spectra of FeCoZr-Al_2O_3 sintered in mixed Ar+O ambient for $X_{FeCoZr} \leq 55$ at.% were evaluated assuming three subspectra: two doublets ($D_1^{Al_2O_3}$: δ=0.08-0.11 mm/s, ε=0.41-0.49 mm/s; $D_2^{Al_2O_3}$: δ=0.40-0.46 mm/s, ε=0.77-0.94 mm/s) associated with Fe^{3+} ions and one doublet assigned to Fe^{2+} state ($D_3^{Al_2O_3}$: δ=0.90-0.96 mm/s, ε=1.81-1.91 mm/s). In accordance with [6] $D_1^{Al_2O_3}$ doublet should be assigned to superparamagnetic FeCoZr nanoparticles separated in Al_2O_3 matrix. $D_2^{Al_2O_3}$ subspectrum has parameters similar to nanosized iron oxides and most probably characterizes oxidized FeCoZr nanoparticles. Basing on magnetometry data as well as electrical conductivity results [6] $D_3^{Al_2O_3}$ doublet may be assigned to complex Fe^{2+} oxides (like $FeCo_2O_4$) formed either on the interface between FeCoZr and Al_2O_3 matrix or inside Al_2O_3 matrix. Mössbauer spectra of samples containing $X_{FeCoZr} > 59$ at. % could be fitted with the superposition of only $D_2^{Al_2O_3}$ and $D_3^{Al_2O_3}$ doublets, while $D_1^{Al_2O_3}$ was not detected. This evidenced that increase of X_{FeCoZr} caused progressive oxidation of FeCoZr nanoparticles and diminishing of residual pure FeCoZr granulas.

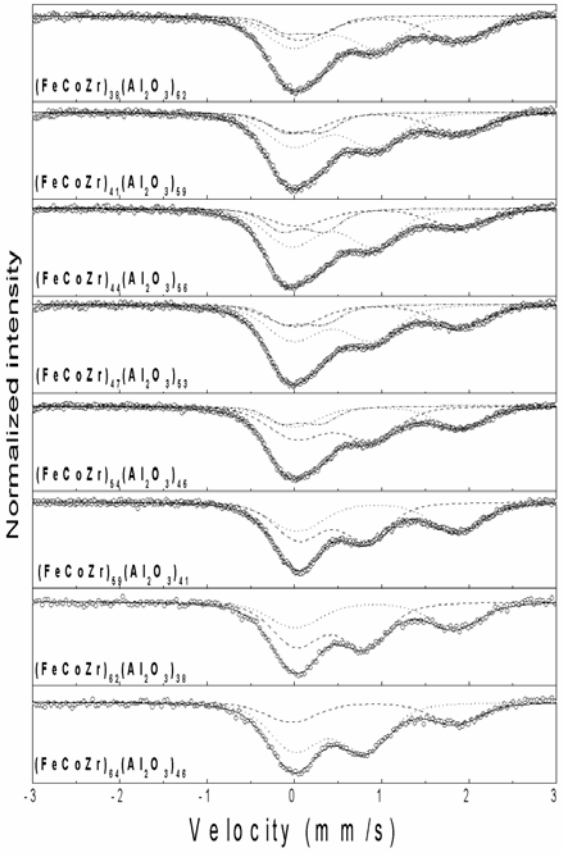

Figure 1 RT Mössbauer spectra recorded for the oxidized FeCoZr-Al_2O_3 films sputtered at $P_O = 4.2 \cdot 10^{-3}$ Pa

2.2. Electrical conductivity and magnetoresistivity

Temperature dependences of DC conductivity $\sigma(T)$ for FeCoZr-Al_2O_3 display, as seen in Fig. 2, activation laws $ln(\sigma) \sim (1/T)^n$ with the "sliding" activation energies at the whole range of X_{FeCoZr}.

As was shown in [7,8] and seen from Fig. 2, $\sigma(T)$ dependences of the most samples studied were close to VRH behaviour

$$\sigma(T) = \sigma_0 \cdot \exp\left(-\left(\frac{T_0}{T}\right)^n\right),$$

where σ_0 is an equilibrium conductivity at $T \to \infty$. In so doing, experiments yielded either the Mott law [7], $ln(\sigma) \propto (T_0^M/T)^{-0,25}$, or the Shklovski-Efros law, $ln(\sigma) \propto (T_0^{SE}/T)^{-0,5}$, where parameters T_0^M and T_0^{SE} determine average activation energies for carrier hopping by localized states around Fermi level in dielectric matrix for Mott and Shklovski-Efros VRH regimes, respectively.

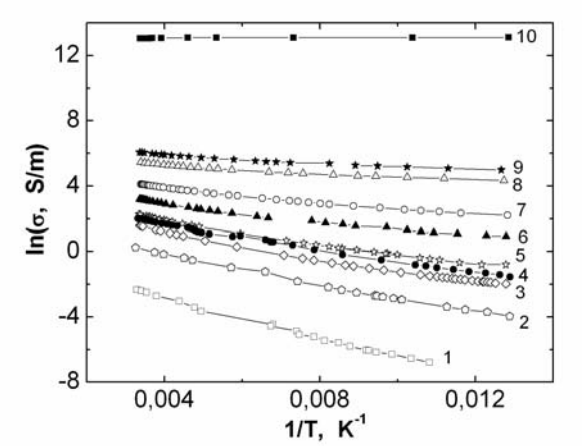

Figure 2 Temperature dependences of conductivity σ(T) for oxidized FeCoZr-Al_2O_3 at X_{FeCoZr} (in at.%) ≈ 31.2 (1), 36.6 (2), 37.4 (3), 38.6 (4), 40.7 (5), 49 (6), 53.6 (7), 62.5 (8), 63.7 (9). Curve 10 - σ(T) for pure FeCoZr

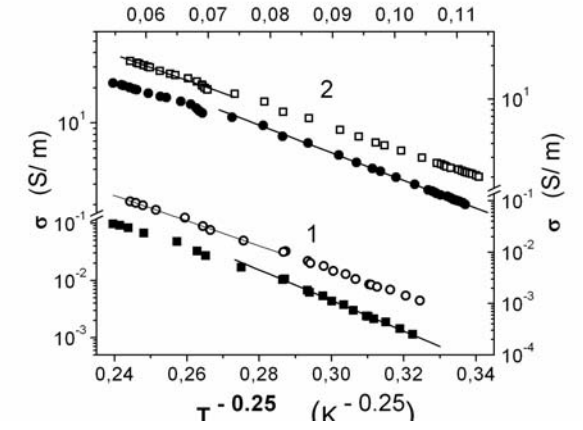

Figure 3 Temperature dependences of conductivity σ (T) for oxidized FeCoZr-Al_2O_3 with x = 31.2 at.% (1) and x = 45 at.% (2)

The fitting procedure for the FeCoZr-Al_2O_3 showed that the Mott law holds only at low temperatures while at higher temperatures T > 160-170 K we observed the crossover from Mott low to the Shklovski-Efros law (see Fig. 3) describing the hopping transport of the charge carriers at the Coulomb gap in the localized states density near Fermi level [9-11].

The activation energies estimated from the σ(T) showed that the T_0^M values are essentially higher by the order of magnitude for the oxidized FeCoZr-Al_2O_3 as compared to the samples sintered in pure Ar [9]. This result strongly correlate with conclusions based on Mössbauer spectroscopy and magnetometry revealing that in the latter case, the oxide "shells", that separate FeCoZr nanoparticles in the current-conducting routes, created additional barriers for electron transport between nanoparticles. Therefore the Shklovski-Efros behaviour of σ(T) in the oxidized FeCoZr can be naturally attributed to the influence of these oxide "shells" possessing semiconductive electric properties [9-11].

The $\sigma(T)$ curves allowed us to estimate principally the changes in the localized state density $N(E_f)$ and localized electron wave function damping length a in Al_2O_3 matrix depending on the X_{FeCoZr} using experimentally extracted T_0 and σ_0 values (see [12]). When the Mott hopping mechanism of VRH carrier transport dominating the semi-empirical Kirkpatrick formula [10]

$$\sigma = 0{,}0217\left(\frac{c}{a}\right)\cdot\left(\frac{T_0}{T}\right)^{0{,}35}\cdot\exp\left[-\left(\frac{T_0}{T}\right)^{0{,}25}\right] = \sigma_{AC}^{o}\cdot\exp\left[-\left(\frac{T_0}{T}\right)^{0{,}25}\right],$$

was used to fit T_0 and σ_0 values, where

$$\sigma_{AC}^{o} \approx \sigma_0\left(\frac{T_0}{T}\right)^{0{,}35}$$

and

$$C = \left(\frac{E_1^2}{\pi^4\cdot d\cdot s^5\cdot\hbar^4}\right)\cdot\left(\frac{2\cdot e^3}{3\cdot 4\cdot\pi\cdot\varepsilon\cdot\varepsilon_0\cdot a}\right)^2.$$

Here a is the localized wave function damping length (in cm), e is the electron charge. The parameters values used in this relations for Al_2O_3 were: deformational potential E_1 = 10 eV, density d = 3.97 g/cm^3, sound velocity s = 3 x 10^3 cm/s, dielectric constant κ_0 = 10 [13]. The σ_0 is constant for the sample (with dimensionality Ω^{-1} cm^{-1}) and $N(E_F)$ – energy density of localized states (eV^{-1}cm$_{-3}$) at the Fermi level in dielectric matrix. Using these parameters we can connect the T_0 and σ_0 values with $N(E_F)$ and a:

$$\sigma_0 = \frac{6.95\cdot 10^{-15}}{a^3},\quad T_0 = \frac{8.65\cdot 10^{-4}}{N(E_F)\cdot a^3}.$$

The estimations of $N(E_F)$ and a values for the case of $X_{FeCoZr} < X_C$ on the base of above presented formulas are shown in Table.

Table

T_0 parameter, equilibrium conductivity σ_0, energy density $N(E_F)$ of localized states at the Fermi level in dielectric matrix and the localized wave function damping length a for oxidized FeCoZr-Al_2O_3 at $T < T_{oc}$ where the Mott law is applied

X_{FeCoZr}, at.%	$T_0\cdot10^{-3}$, K	$\sigma_0\cdot10^{-3}$, S/m	a, nm	$N(E_F)\cdot10^{-18}$, eV^{-1}cm^{-3}
31.2	1990	12390	4	144
36.6	795	5318	5	213
37.4	323	976	8	131

As follows from the Table in the range of 31 < X_{FeCoZr} < 40 at.% (below the percolation threshold X_C) radius of localization of electrons is about 9 ± 2 nm and $N(E_F)$ is about (3 ÷12)·10^{18} $eV^{-1}cm^{-3}$. The addition of oxygen to Ar ambient of sputtering chamber results in some lowering of a down to 6 ±2 nm and the increase of $N(E_F)$ up to (1 ÷2)·10^{20} $eV^{-1}cm^{-3}$ (see, Table). This increase of $N(E_F)$ nearly 2 orders in the FeCoZr-Al_2O_3 films can be attributed to the influence of oxide "shells" around FeCoZr nanoparticles.

Additional confirmation of tunnelling and/or VRH mechanisms of carrier transport was obtained from the investigation of magnetoresistive effect in the studied nanocomposite films. The DC measurements at room temperature for oxidized FeCoZr-Al_2O_3 showed (see Fig. 4) that the magnetoresistance $r(B) = (\Delta\rho(B)/\rho(0))$ of the studied nanocomposites films was negative and obeyed the relationship of $r(B) \propto - B^k$ as the magnetic induction B increased.

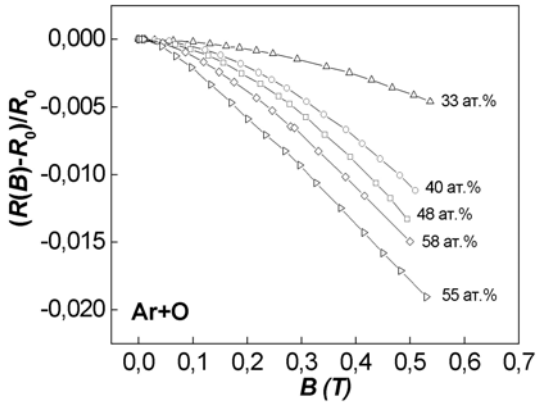

Figure 4 Reduced resistance vs magnetic induction B at RT for oxidized FeCoZr-Al_2O_3

3. STRUCTURE AND PROPERTIES OF FeCoZr-PZT SINTERED IN Ar+O AMBIENT

3.1. Mössbauer spectroscopy

Mössbauer spectra of selected granular nanocomposite films $(FeCoZr)_X(PZT)_{100-X}$ sintered at lower (P_O = 2,4·10^{-3} Pa) and higher (P_O = 3,7·10^{-3} Pa) oxygen pressure are shown in Figs. 5 and 6. It appeared that at lower P_O Mössbauer spectroscopy revealed the transition from nonmagnetic spectra towards superposition of magnetically split sextets and nonmagnetic subspectra around X_{FeCoZr} = 51 at. %. More particularly, spectra of $(FeCoZr)_{28}(PZT)_{72}$ and $(FeCoZr)_{38}(PZT)_{62}$ (not shown here) were fitted with two doublets (D_2^{PZT} and D_3^{PZT}). Parameters of the D_2^{PZT} doublet (δ=0.32 mm/s, ε=0.96 mm/s) are quite close to those of $D_2^{Al_2O_3}$. This suggests that D_2^{PZT} is related to Fe^{3+} ions located in oxidized FeCoZr nanoparticles. Assuming similarity of $D_3^{Al_2O_3}$ and D_3^{PZT} (δ=0.97 mm/s, ε=1.72 mm/s) the latter may characterize Fe^{2+} ions either on the interface between FeCoZr and PZT matrix or inside PZT matrix.

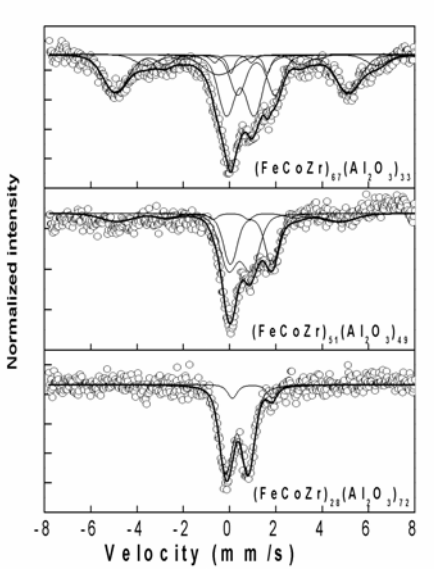

Figure 5 Mössbauer spectra of selected granular oxidized nanocomposite films $(FeCoZr)_X(PZT)_{100-X}$ sintered at P_O = 2,4·10^{-3} Pa

Drastic change of Mössbauer spectra was observed for FeCoZr-PZT containing X_{FeCoZr} = 51 at. %. At this composition additional magnetically split sextet S_1^{PZT} (H_{hf}=29.9 T) appeared. In correlation with data reported for FeCoZr-Al_2O_3 in [8, 14] X_{FeCoZr} = 51 at. % may be considered as a threshold concentration for the formation of ferromagnetically interacting net of FeCoZr nanoparticles. Insufficient increase of H_{hf} (up to 31.2 T for $(FeCoZr)_{67}(PZT)_{23}$) and evident growth of S_1^{PZT} contribution at the expense of D_2^{PZT} and D_3^{PZT} were observed with further increase of X_{FeCoZr}.

Mössbauer spectra of FeCoZr-PZT sintered at higher (P_O = 3,7·10^{-3} Pa) pressure (see Fig.6) revealed only Fe^{3+} doublet (δ=0.30-032 mm/s, ε=0.98-1.03 mm/s) evidencing the formation of oxidized FeCoZr nanoparticles in the whole range of studied X_{FeCoZr}.

It should be mentioned that the basic peculiarity of FeCoZr-PZT samples was absence of residual nonoxidized FeCoZr nanoparticles for the cases of both P_O values (2.4·10^{-3} Pa and 3,8·10^{-3} Pa).

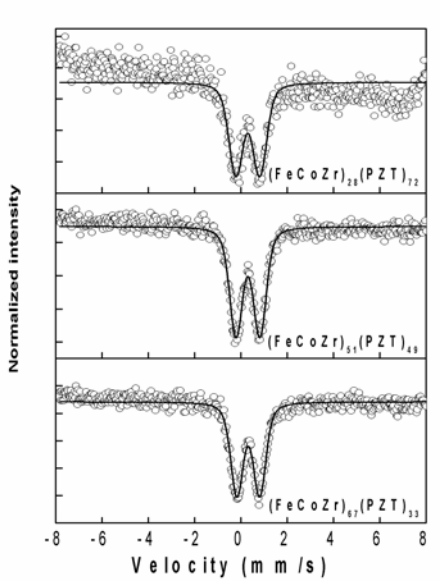

Figure 6 Mössbauer spectra of selected granular oxidized nanocomposite films $(FeCoZr)_X(PZT)_{100-X}$ sintered at $P_O = 3{,}8 \cdot 10^{-3}$ Pa

3.2. Electrical conductivity and magnetoresistivity

Electrical resistivity ρ of FeCoZr-Al_2O_3 and FeCoZr-PZT films revealed principally different behavior both with X_{FeCoZr} (Fig. 7) and temperature T (see, Figs. 8 and 9). As is seen from comparison of ρ(x) dependences in Fig. 7, FeCoZr-Al_2O_3 films (both oxidized and nonoxidized) showed monotoneous drop of ρ(x) (curves 1-2 in Fig. 7) while for FeCoZr-PZT nanocomposites ρ(x) possesses "plateau" at X_{FeCoZr} > 42-45 at.%.

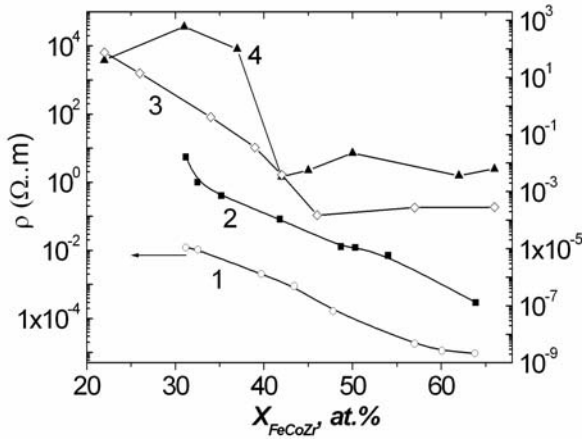

Figure 7 Dependences ρ(x) for the films FeCoZr-Al_2O_3 sintered in pure Ar (curve 1) and in mixture Ar + O_2 at $P_O = 4{,}1 \cdot 10^{-3}$ Pa (curve 2), for FeCoZr-PZT sintered in mixture Ar + O_2 at $P_O = 2{,}4 \cdot 10^{-3}$ Pa (curve 3) and at $P_O = 3{,}8 \cdot 10^{-3}$ Pa (curve 4)

Remember also that FeCoZr-Al_2O_3 (deposited at P_O = $4{,}1 \cdot 10^{-3}$ Pa) and FeCoZr-PZT deposited at close pressure (P_O = $3{,}8 \cdot 10^{-3}$ Pa) revealed no formation of current-conducting (percolative) cluster as well as ferromagnetically interacting net of FeCoZr or FeCo-based oxide nanoparticles beyond the percolation threshold X_C ≈ 43-45 at.% for FeCoZr-Al_2O_3 deposited in pure Ar (at P_O = 0). This was in strong correlation with tunneling and/or VHR carrier transport mechanism for the samples FeCoZr-Al_2O_3 with x > 45 at.% observed in [6]. We believe that this conservation of activational conductivity is due to FeCoZr nanoparticles covered with oxide "shells" which also prevent their ferromagnetic coupling.

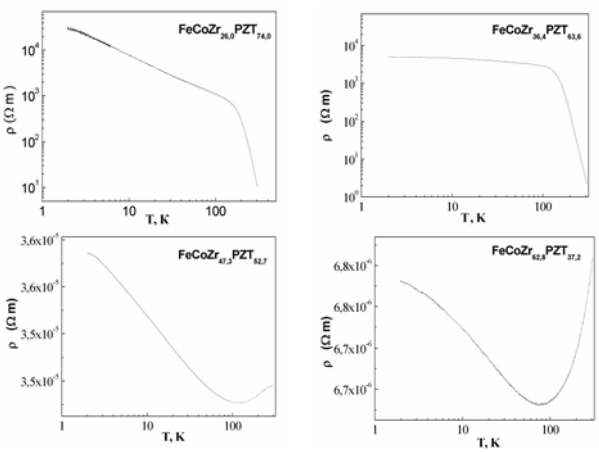

Figure 8 Temperature dependencies of electrical conductivity ρ(T) in lgρ - lgT scale for FeCoZr-PZT GNC sintered at $P_O = 2.4 \cdot 10^{-3}$ Pa

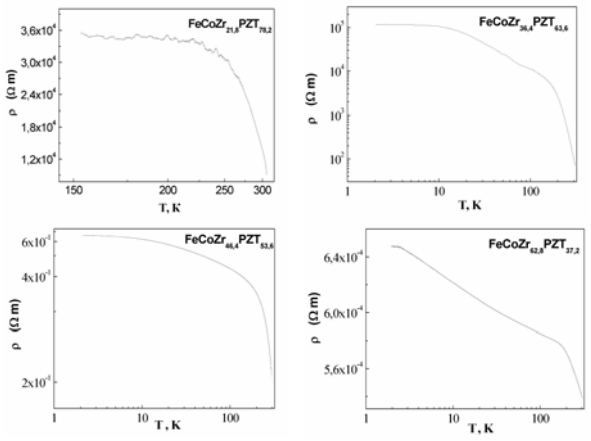

Figure 9 Temperature dependencies of electrical conductivity ρ(T) in lgρ - lgT scale for FeCoZr-PZT GNC sintered at $P_O = 3.8 \cdot 10^{-3}$ Pa

Temperature dependencies of electrical conductivity ρ(T) of FeCoZr-PZT sintered in at P_O = $2.4 \cdot 10^{-3}$ Pa and $3.8 \cdot 10^{-3}$ Pa are presented in Figs. 8 and 9, correspondingly. Obtained curves revealed quite different change with X_{FeCoZr} increase for both applied P_O values and also as compared to FeCoZr-Al_2O_3 [6]. It was previously suggested (see Fig. 3) that ρ(T) of FeCoZr-Al_2O_3, sintered at P_O = $4{,}1 \cdot 10^{-3}$ Pa was quite typical for VHR conductivity by Mott and Shklovski-Efros laws. Although ρ(T) observed for FeCoZr-PZT possessed negative temperature

coefficient of resistivity dρ/dT, in majority of compositions ρ(T) cannot be fitted within assumption of VHR Mott conductivity (curves are not linear in Mott scale, see Fig. 3). As evidenced from Figs. 8 and 9 ρ(T) curves for FeCoZr-PZT can be fitted with straight lines only in double logarithmic scale that is typical rather for power-like law.

For $(FeCoZr)_{47}(PZT)_{53}$ and $(FeCoZr)_{62,8}(PZT)_{37,2}$ samples sintered at lower P_O ($2.4 \cdot 10^{-3}$ Pa) the transition from negative to positive dρ/dT value at T > 100 K (see Fig. 8) should be assigned to some contribution of metallic conductivity in strong correlation with Mössbauer data (see Fig. 5) evidencing the formation of ferromagnetically interacting net of FeCoZr nanoparticles.

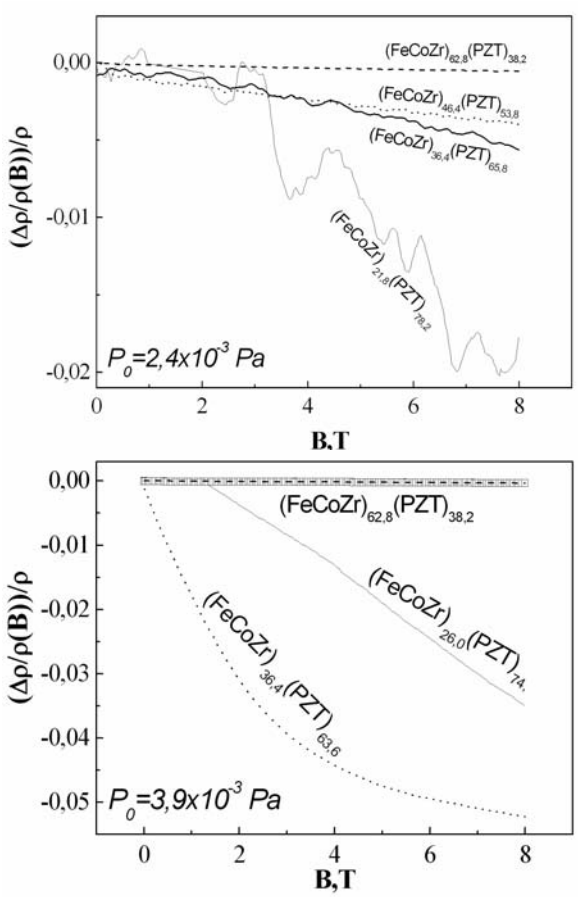

Figure 10 Reduced resistances vs magnetic induction B at RT for nanocomposite films FeCoZr-PZT sintered at $P_O = 2.4 \cdot 10^{-3}$ Pa and $3.8 \cdot 10^{-3}$ Pa.

Similarly to the case of FeCoZr-Al_2O_3 GNC negative sign of $\Delta\rho(B)/\rho(0)$ for FeCoZr-PZT (see Fig. 10) supported the superposition of tunneling and VHR conductivity mechanisms. Contributions of both conductivity channels should vary with change of FeCoZr and PZT fractions.

4. SUMMARY

Mössbauer spectroscopy revealed some peculiarities in oxidation of FeCoZr nanogranules in FeCoZr-PZT GNCs as compared to FeCoZr-Al_2O_3 *GNC*. Contrary to the case of FeCoZr-Al_2O_3 *GNCs*, FeCoZr nanogranules in FeCoZr-PZT sintered both at $P_O = 2.4 \cdot 10^{-3}$ Pa and $3.8 \cdot 10^{-3}$ Pa seemed to be totally oxidized in the whole range of X_{FeCoZr} values. In the case of FeCoZr-Al_2O_3 *GNCs* subspectrum, attributed to nonoxidized FeCoZr granules was detected up to $X_{FeCoZr} \approx 55$ at.%. Such a difference evidences the effect of matrix (Al_2O_3 and PZT) on the formation of FeCoZr oxides. One may suggest that oxidation of FeCoZr nanoparticles in FeCoZr-Al_2O_3 at $X_{FeCoZr} < 55$ at.% may be slowed down with chemically inert and resistant to oxidation Al_2O_3 matrix.

Another specific feature of FeCoZr-PZT (deposited at higher $P_O = 3.8 \cdot 10^{-3}$ Pa is only one formed Fe^{3+} configuration characteristic to oxidized FeCoZr nanoparticles to in the whole X_{FeCoZr} range. FeCoZr-Al_2O_3 sintered at close $P_O = 4.2 \cdot 10^{-3}$ Pa definitely showed quite large paramagnetic Fe^{2+} contribution.

Change of σ(T) observed for FeCoZr-PZT sintered at $P_O = 2{,}4 \cdot 10^{-3}$ Pa (see Fig.8) evidenced the metallic conductivity channel at X_{FeCoZr} above ≈ 47 at. % in strong correlation with Mössbauer data (see Fig. 5) evidencing the coupling of FeCoZr nanoparticles at $X_{FeCoZr} \approx 51$ at %.

Deviations of σ(T) of FeCoZr-PZT sintered at $P_O = 3{,}8 \cdot 10^{-3}$ Pa from Mott's law (Fig. 9) as well as untypical shape of σ(x) curve as compared to FeCoZr-Al_2O_3 (Fig. 8) cannot be confidently explained and assigned to transformation of FeCoZr nanoparticles state. With regard to almost unchanged Mössbauer spectra of FeCoZr-PZT (see Fig. 6) peculiar behavior of σ(x) and σ(T) should be related to the electric properties of PZT matrix rather than to the variation of FeCoZr state with X_{FeCoZr}.

5. REFERENCES

[1] W. Li, Yu. Sun, C.R. Sullivan, "High-frequency resistivity of soft magnetic granular films", IEEE Trans. Magn., Vol. 41, pp. 3283-3285, 2005.

[2] C.R. Sullivan, S. Prabhakaran, P. Dhagat, Y. Sun, "Thin-film inductor designs and materials for high-current low-voltage power", Trans. Magn. Soc. Japan. , Vol.3, pp.126-128, 2003.

[3] P. Dhagat, S. Prabhakaran, C.R. Sullivan**,** "Comparison of magnetic materials for V-groove inductors in optimized high-frequency DC-DC converters", IEEE Trans. Magn., Vol.40, pp. 2008-2010, 2004.

[4] D.Stauffer, A.Aharony, Introduction to percolation theory, Taylor and Francis, London, 1992.

[5] J. Fedotova et al, "The effect of the sputtering process ambient on the magnetic state and phase composition of the film nanocomposites $(Fe_{0.45}Co_{0.45}Zr_{0.10})_x(Al_2O_3)_{1-x}$", Hyper. Inter., Springer, 165 (1-4), pp. 127-134, 2005.

[6] J.A.Fedotova. "FeCoZr-Al_2O_3 granular nanocomposite films with tailored structural, electric, magnetotransport and magnetic properties", "Advances in Nanoscale Magnetism", Chapter 13, Springer, pp. 231-367, 2008.

[7] N.F. Mott, E.A. Devis, Electron processes in noncrystalline materials. Claredon Press, Oxford, 1979.

[8] A. Saad, A. Fedotov, I. Svito, A. Mazanik, B. Andrievski, A. Patryn, Yu. Kalinin, A. Sitnikov, "AC conductance of $(Co_{0.45}Fe_{0.45}Zr_{0.10})_X(Al_2O_3)_{1-X}$ nanocomposites", Progr. in Solid. State Chem., Elsevier, pp. 139-146, 2006.

[9] A. Saad, A. Mazanik, Yu. Kalinin, J. Fedotova, A. Fedotov et al, "Structure and electrical properties of CoFeZr-aluminium oxide nanocomposite films", Adv. Mater. Sci., Elsevier, pp. 34-40, 2004.

[10] K. Yasuda, A. Yoshida, T. Arizumi, "The effects of annealing on Mott's parameters for hopping conduction in amorphous Ge", Phys. Stat. Sol., Wiley, (a), pp. K181-K184, 1977.

[11] J. Inoe, S. Markava, "Theory of tunneling magnetoresistance in granular magnetic films", Phys. Rev. B, AIP, pp. R11927-R11929, 1996.

[12] A.M. Saad, B. Andrievsky, A. Fedotov, J. Fedotova, T. Figielski, Yu. Kalinin, et al, "AC and DC carrier transport in $(CoFeZr)_x(Al_2O_3)_{1-x}$ nanocomposite films for spintronic applications", Proc. 1st Int. Workshop on Semiconductor Nanocrystals (Seminano2005) September 10-12, 2005, Budapest, Hungary, pp. 321-324, 2005.

[13] A.P. Babichev, N.A. Babushkina, Physical Units, Moscow, 1991.

[14] A.M. Saad et al. "Structure and magnetic properties of nanogranular composites CoFeZr-alumina", Rev. Adv. Mater. Sci., Elsevier, 14, pp. 14-34, 2007.